Diamond Chemical Vapour Deposition using a zero-total gas flow environment

A, Croot[2], E.J.D. Mahoney[1], H. Dominguez-Andrade[2], M.N.R. Ashfold[1] and N.A. Fox*[1, 2],

[1]School of Chemistry, University of Bristol, Cantocks Close, Bristol, BS8 1TS, UK

[2]School of Physics, University of Bristol, Tyndall Avenue, Bristol, BS8 1TL, U.K.

Corresponding author: Dr Neil A Fox, neil.fox@bristol.ac.uk, Tel. 44+117 928 8729

Diamond Chemical Vapour Deposition using a zero-total gas flow environment

Abstract

We demonstrate diamond growth through microwave plasma-enhanced chemical vapor deposition using a sealed (static-mode) CH_4/H_2 process gas mixture. The growth experiments were complemented by spatially and spectrally resolved optical emission imaging measurements of electronically excited C_2 and CH radicals in the hot plasma core. The as-grown material was characterized by Raman Spectroscopy and Scanning Electron Microscopy and shown to be typical of polycrystalline diamond grown using traditional methods. Moreover, this material was essentially indistinguishable from material grown using a tracked flow-mode of operation in which the input methane flow rate was progressively reduced to mimic the time evolving C_2 emission intensities in the static-mode experiments. These proving static-mode studies demonstrate a ~30-fold improvement (*cf.* that achieved using standard flow-mode conditions) in the conversion efficiency of carbon in the input source gas into diamond, and we argue that further gains should be possible with appropriate reactor and process optimization. Static-flow growth could be particularly advantageous in the case of depositions using limited, expensive, hazardous, or environmentally damaging feedstock gases.

Keywords:

Diamond; Microwave; Zero-flow Process Gas; Optical Emission Spectroscopy; Laser Raman Spectroscopy; Scanning Electron Microscopy.

1. Introduction

Diamond boasts a range of outstanding properties fit for 21st century technological applications. Its high thermal conductivity and low thermal expansion coefficient make diamond an extremely good material for thermal management in electronics, whilst its high refractive index, low birefringence and exceptionally broad optical transparency make it applicable for optical windows and desirable as a lasing material.[1-7] Additionally, diamond is a wide band-gap material which, upon boron doping, can demonstrate p-type semiconducting, metallic or superconducting behaviour, facilitating its use as an active component in electronic applications.[8]

Chemical vapor deposition (CVD) methods can be used to produce diamond films with morphologies ranging from nano- to micro- polycrystalline through to larger high-quality single crystal diamonds.[9,10] This is achieved by flowing methane diluted (to just a few percent) with hydrogen into a growth chamber. The gas mixture is activated, most commonly by a microwave (MW) plasma.[1,7,9,10] The processes occurring within MW activated C/H plasmas that facilitate diamond growth are by now reasonably well understood, [7,11-15] as are the conditions required to ensure suitably high densities of the species important for growth (notably CH_3 radicals and H atoms) directly above the growing surface.[7,11-15] Many of the key processes occurring in MW activated C/H/N [16] and C/H/O [17] plasmas are similarly reasonably well understood, as are at least some of the effects that that both O and N can have on diamond growth rate, crystal quality and morphology.[18-25] The presence of trace amounts of oxygen and nitrogen generally lead to an increase in diamond growth rate but to the detriment of quality,[18-25] with nitrogen encouraging the growth of (100) facets and twinning along the (111)-orientation. [21,22]

Traditional diamond CVD uses a premixed source gas. A stable process pressure (that is almost always below atmospheric pressure) is achieved by matching the gas input and exhaust flow rates. The residence time is defined as the time taken to replenish the entire gas content of the chamber up to the pressure selected for growth. Prior investigations of the effects of gas flow rate on diamond growth rates and morphology have yielded contradictory findings.[26--32]

Celii *et al*., for example, reported MW plasma activated diamond CVD growth studies (on both Si and diamond substrates) in which the residence time was varied by more than a factor of thirty.[28,29] While Raman, photoluminescence (PL) and X-ray diffraction data for the as-grown material all showed some sensitivity to the gas flow rate employed, other material properties (electrical resistivity, IR transmission, deposited film thickness) and the optical emission spectra of the plasma were found to be rather insensitive to the flow rate. Flow modelling suggested the importance of convective flow at the low pressures (40 Torr) used in that study, and the authors argued that the presence of vortices above the growing diamond surface likely complicated the concept of residence time for their experiments. There appears to be no clear consensus as to how, or even if, flow rate substantially impacts growth rate.[28-30]

Trace amounts of air enter the CVD process either as an impurity in the input source gas mixture or via small leaks into the reactor volume. The use of higher flow rates (shorter residence times) should reduce the relative importance of any such contribution from reactor leaks. Such expectations are consistent with studies by Nistor *et al.*,[31] for example, who demonstrated a decrease in N-related defects in material grown at higher gas flow rates, and by Su *et al*.,[30] who reported increased quality and reduced growth rates when using relatively higher flow rates (in the low-flow regime). However, if low (or ideally zero) leak rates can be achieved, increasing the gas residence time could be desirable from the perspectives of reducing diamond production costs or mitigating health and safety issues when using expensive, rare, toxic or even radioactive source gases. There are prior reports [33,34] (and patents [35]) describing process gas recycling in diamond CVD systems but we have not found any prior report describing CVD growth using a sealed gas sample (*i.e*. growth at zero gas flow rate).

Here we show successful diamond CVD from a MW activated sealed C/H gas sample, using what we term a "static-mode" plasma. The demonstration involves comparison with diamond samples grown using the same MW reactor working in the standard "flow-mode" (*i.e*. CVD with a flowing gas sample, and residence times ~2 min). In addition to material comparisons based on Raman Spectroscopy and Scanning Electron Microscopy (SEM) measurements, the present study also employed Optical Emission Spectroscopy (OES) to track emitting C_2 and CH species during growth from both the static- and flow-mode C/H plasmas. Prior studies have demonstrated that the C_2(d−a) emission intensity from the hot plasma core region is a good proxy for the local C content in that region,[30,36,37] while the CH(A−X) emission intensity is the

better signifier of the concentrations of the CH_x ($0 \leq x \leq 3$) species implicated in diamond growth.[32]

2. Experimental methods

Prior to diamond growth, 10 mm^2 silicon substrates of thickness 0.5 mm ([100]; p-type; PiKEM, UK), were seeded using a two-step process described elsewhere[38].

MW CVD was performed using a reactor that has also been described previously.[36] For future reference, the volume of the cylindrical reactor was ~600 cm^3, but the valve on the exit side of the reactor was at the end of a long manifold, close to the pump; the total volume in static-mode operation was ~2.5 L (estimated by a pressure-rise test using the calibrated H_2 mass flow controller).

In standard flow-mode operation, P = 1.5 kW of (2.45 GHz) MW power was supplied to the chamber maintained at a pressure p = 150 Torr of hydrogen (purity N7; generated by electrolyzing (Milli-Q purified) water; Noblegen MicroPROGEL, UK) and methane (N5.5; Air-Liquide, UK). Gas flow rates, $F(H_2)$ = 300 standard cm^3 min^{-1} (sccm) and $F(CH_4)$ = 19 sccm resulted in a process gas mixture of 6% methane in hydrogen. The Si substrate was positioned axially symmetrically on a tungsten disk (1.25" diameter, 3 mm thick) which was separated from the water-cooled aluminum base-plate of the reactor by an annular molybdenum wire spacer with user-selectable diameter in the range $0.002" \leq d_{wire} \leq 0.006"$. Varying the spacer wire diameter enabled some variation of the substrate temperature, T_{sub}, while causing minimal change to the plasma parameters.

The static-mode plasmas were initially ignited in p = 15 Torr of pure H_2. The valve in the pumping line was then shut, simultaneously with the opening of the CH_4 and H_2 (6% mixing ratio) flows, thereby ensuring that no methane was lost before deposition conditions were reached. Once p = 150 Torr, the CH_4 and H_2 gas flows were switched off. This point was taken as t = 0 when defining growth times in static-mode operation. Given that the plasma ignition pressure was 10% of the eventual deposition pressure, the initial input methane mole fraction for the static deposition runs was 5.4%. Both static- and flow-mode depositions were run to a maximum time t = 90 min.

The intensities of the $C_2(d^3\Pi_g - a^3\Pi_u)$ $\Delta v = 0$ and $CH(A^2\Delta - X^2\Pi)$ $\Delta v = 0$ emissions, henceforth referred to as $I(C_2^*)$ and $I(CH^*)$ respectively, were imaged using a Czerny-Turner spectrograph (Shamrock SR-303i-A, Andor, UK) equipped with a 500 mm focal length, f/5.6 objective lens.

After passing through a ~10 μm vertical slit the emissions are dispersed by a 1200 grooves per mm diffraction grating, yielding a spectral resolution of ~ 0.09 nm (Full Width at Half Maximum, FWHM) when imaged by a cooled CCD detector (Newton DU970PBV, Andor, UK). The samples were analysed first by Raman spectroscopy (2000 series, Renishaw, UK) using a 514.5 nm Ar ion laser (Excelsior series, Spectra-Physics, UK), and then by SEM (Sigma, Zeiss, Germany), which required sputter deposition of a thin (~ 20 nm) gold layer to mitigate charging effects. The combination of Raman spectroscopy and SEM analysis yields film quality and thickness information. The latter was measured at a range of points across each sample in a set of four cross-sectional images, the locations of which on the film surface form a square of side length 4 mm, centred at the middle of the sample. Two linear cleaves, 4 mm apart (i.e., 3 mm from the sample edge), were required to expose these points for examination.

3. Results and Discussion

A total of six static-mode growth experiments were carried out, four of which investigated the effect of T_{sub} (using different spacer wire thicknesses to yield T_{sub} ~ 765, 830, 890 and 950 °C) for a growth time t = 90 min. The other two were shorter growth runs performed at T_{sub} ~ 890 °C, for t = 30 and 60 min respectively. When combined with the T_{sub} ~ 890 °C, t = 90 min experiment, these allowed investigation of how the growth rate evolved with time at a common T_{sub}. The reactor leak rate (which, as noted above, is another parameter that could influence film deposition rate and morphology) was measured prior to each growth experiment by evacuating the reactor, closing the valve to the pump and monitoring the pressure rise over a 60 min period.

The emission intensities, $I(C_2^*)$ and I(CH*), were monitored during each growth experiment. Figure 1 shows a sample image of the C_2(d−a) Δv = 0 system. Data were extracted and processed using the PGOPHER software package[39] to simulate and integrate the entire emission intensity in each spectrum (or just the emission intensity at a chosen range of heights z above the substrate), with proper consideration of T_{gas} and the spectral resolution, in order to provide a relative emission $I(C_2^*)$ (or I(CH*)) intensity at any time within each deposition run. The emitting species are generated by electron impact excitation of the corresponding ground state species (in the case of CH or, in the case of C_2, of radicals in the low lying $a^3\Pi_u$ state also), supplemented by chemiluminescent bimolecular reactive sources.[40] The measured OES intensities are thus sensitive to the product of the local concentrations of the lower state species

of interest and of suitably energetic electrons.[7,37] The electron energy distribution function at any given location within the reactor is assumed to be essentially constant during any particular growth run. Thus the (relative) OES intensity gives a measure of the relevant species concentration and its evolution within (and between) experiments and normalizing to the highest intensity in any static-mode dataset, generally at t = 0 min, allows easy comparison between deposition experiments.

For comparison purposes, two depositions were also carried out starting from the flow-mode conditions described above, with $F(CH_4)$ = 19 and 17 sccm respectively and T_{sub}~ 885 °C. $F(CH_4)$ was decreased manually in a stepwise fashion (specified later) during the full 90 min growth period, so as to mimic the declining gas phase carbon content (estimated via the $I(C_2^*)$ signal from the hot plasma core) during static-mode growth.

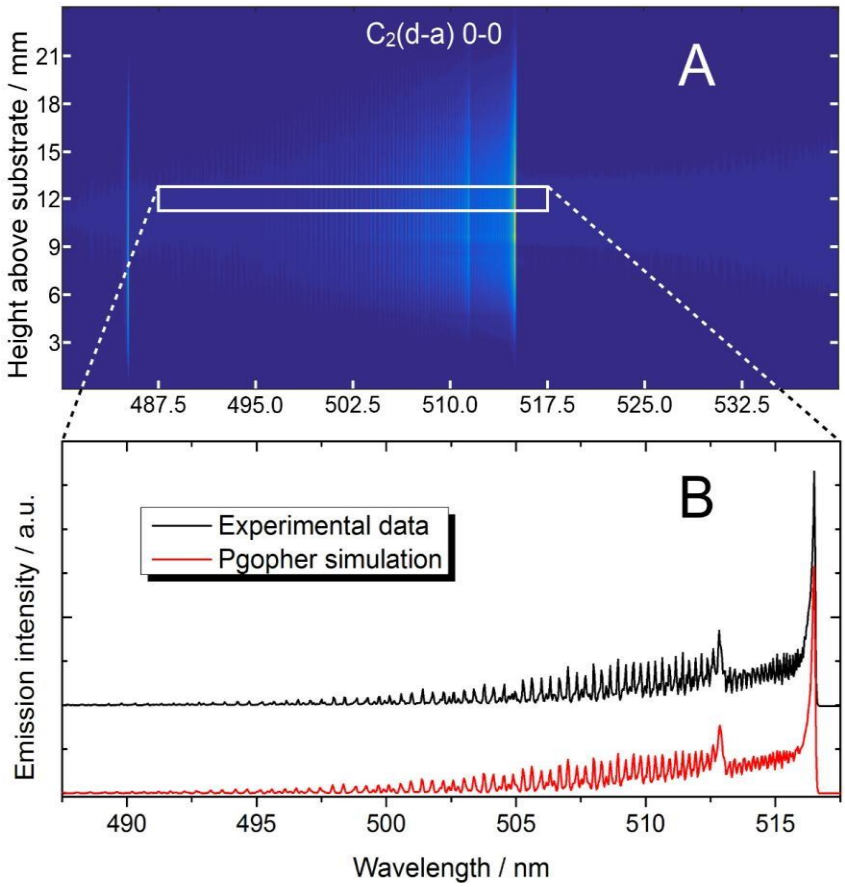

Figure 1: (A) Spatially and spectrally resolved image of optical emission in the wavelength region that includes the C_2(d−a) Δv = 0 system and the H-Balmer α line at 486 nm. (B) Spectrum of intensity versus wavelength for emission from the region z = 12 ± 0.75 mm above the substrate surface (indicated by the white rectangle in (A)), along with the PGOPHER simulation.

3.1 Time-dependent $I(C_2^*)$ and $I(CH^*)$ optical emission intensities in static-mode

As Figure 2 shows, I(C_2^*; z ~ 12 mm) and I(CH*; z ~ 12 mm) both decline during the entire 90 min static-mode growth experiments, at rates that increase with increasing T_{sub}. Analysis of these emission data at other z show very similar trends: The $I(C_2^*)$ intensity declines exponentially with a time constant, τ, that scales inversely with T_{sub}. The I(CH*) intensity drops less steeply and, even at the highest T_{sub} investigated, had only declined to ~40% of its initial value by t = 90 min. These differences are reminiscent of the results of previous flow-mode studies of the ways in which the C_2 and CH concentrations in the plasma vary with changes in $F(CH_4)$.[37] This finding suggests that $I(C_2^*)$ remains a good proxy for the total C content in the plasma region under static-mode conditions and that we might expect a correlation between the rate of fall of $I(C_2^*)$ and the material deposition rate.

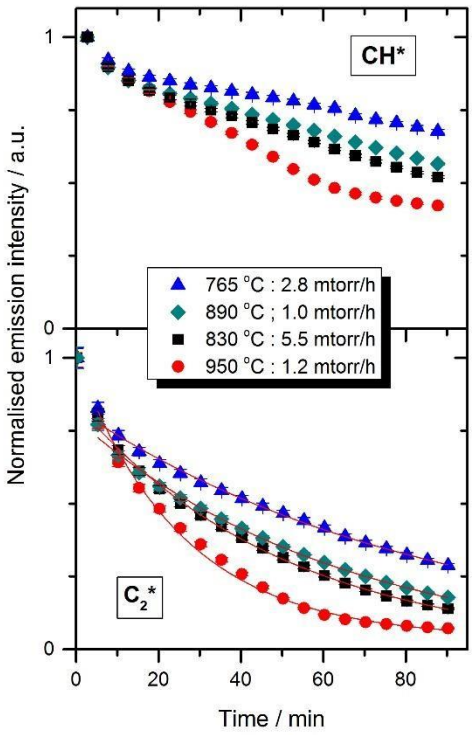

Figure 2: I(CH*) and $I(C_2^*)$ emission intensities measured as a function of time during static mode growth at four different substrate temperatures (shown in the legend, along with the reactor leak rate measured immediately prior to that particular growth run). The solid lines in the lower panel are fitted exponential decays from the second (t = 3 min) data point onwards, by which time the plasma is considered to have reached quasi-steady state.

3.2 **Correlation between deposition rate and decay constant of the *I*(C_2*) emission intensity in static mode conditions**

The correlation between *I*(C_2*) and the deposition rate is confirmed by Figure 3, which compares the deposited material thickness after growth for *t* = 90 min (as determined by cross-sectional SEM) with the corresponding *I*(C_2*; *z* ~ 12 mm) decay constant for three different growth temperatures. The SEM images shown in the insets to this figure show the facetted morphology expected of polycrystalline diamond, the quality of which is assessed later. As noted previously, the relatively small changes in T_{sub} are expected to have minimal influence on the plasma processing and plasma parameters in the plasma core but will influence the gas-surface chemistry required for growth and thus the rate of loss of carbon from the plasma to the substrate. The measured trends suggest that deposition on the substrate is a significant sink for gas phase C under static-mode conditions.

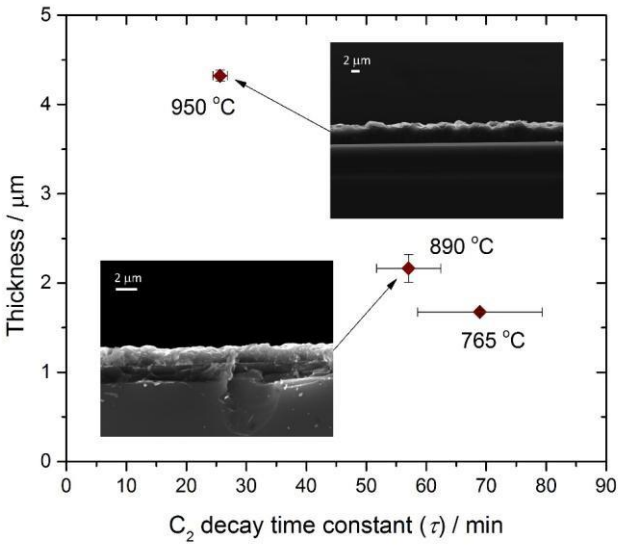

Figure 3: Plot of deposited film thickness following static-mode deposition for *t* = 90 min against the decay constant of the *I*(C_2*) emission. Representative cross section SEM images of the samples grown at T_{sub} = 890 and 950°C are shown in the insets and the bars on the data points represent the standard error.

Figure 4 shows how the thickness of diamond samples grown under static-mode conditions at similar T_{sub} values (~880°C) and with similar reactor leak rates (low, ~1 mtorr/h) scales with deposition time. These data reveal a relatively constant growth rate throughout the whole *t* =

90 min, notwithstanding the inevitable decline in the C content of the plasma. As Figure 2 showed, at T_{sub} ~880°C, $I(C_2^*)$ in the plasma core has dropped to ~30% of its initial value by t = 60 min. The small variations in T_{sub} between these three experiments may have a minor influence on the thickness comparison, but the fact that the growth rate appears undiminished at later times serves to remind us of the complexity of the gas phase and gas-surface chemistry that drives diamond CVD. The rates of the gas phase coupling reactions between C_2H_y ($0 \leq y \leq 6$) and CH_x ($0 \leq x \leq 4$) species, and thus the absolute concentrations of these various species, depend on many factors including the local C/H ratio, T_{gas} and therefore the location within the reactor volume. One key factor in diamond CVD is the concentration of CH_x species in the immediate vicinity of the substrate. As Figure 2 shows, $I(CH^*; z \sim 12$ mm) declines more slowly than $I(C_2^*; z \sim 12$ mm). Prior plasma chemistry modelling (of flow-mode conditions) [16,17,37] shows that this trend extends to small z and that addition reactions involving CH_x species (particularly CH_3 radicals) are important in diamond growth. Thus, it is unsurprising that growth continued at later times but, clearly, growth must cease when the reservoir of gas phase carbon is fully depleted. We return to discuss this issue further later, when comparing flow- and static-mode growth.

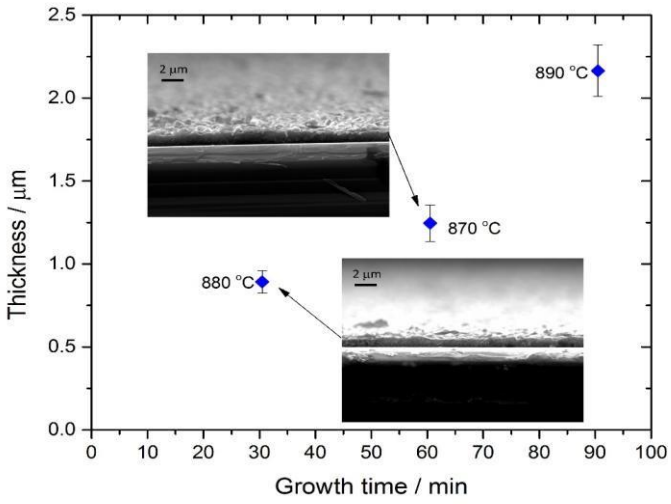

Figure 4: Diamond thickness as a function of deposition time for three samples grown at very similar deposition temperatures, T_{sub}. Representative cross section SEM images of the t = 30 and t = 60-min samples are shown in the insets and the bars on the data points represent the standard error.

3.3 Raman spectroscopy of the diamond deposited under static mode conditions

Raman spectroscopy (λ = 514.5 nm excitation) was used to confirm the presence and quality of the as-grown diamond samples. As Figure 5 shows, the Raman spectra measured from all of the static-mode deposited samples are dominated by the 1332 cm^{-1} sp^3 carbon peak and are characteristic of polycrystalline diamond. Since the deposits are polycrystalline, each sample has some inherent sp^2 carbon in the grain boundaries – which is revealed by the features at ~1140 cm^{-1} and in the 1400-1650 cm^{-1} region. These sp^2 features are more prominent in the spectra of films grown for shorter time durations and in films grown at lower T_{sub} (~765°C), where the grain size is clearly smaller. The Raman spectrum of the sample grown with a higher reactor leak rate (T_{sub} ~ 830°C; 5.5 mtorr h^{-1}) also shows a higher graphitic carbon content – consistent with an enhanced re-nucleation rate in the presence of N_2.[18,21] Each of the foregoing observations mimic trends found with standard flow-mode diamond CVD, implying that there are few fundamental differences between flow- and static-mode growth.

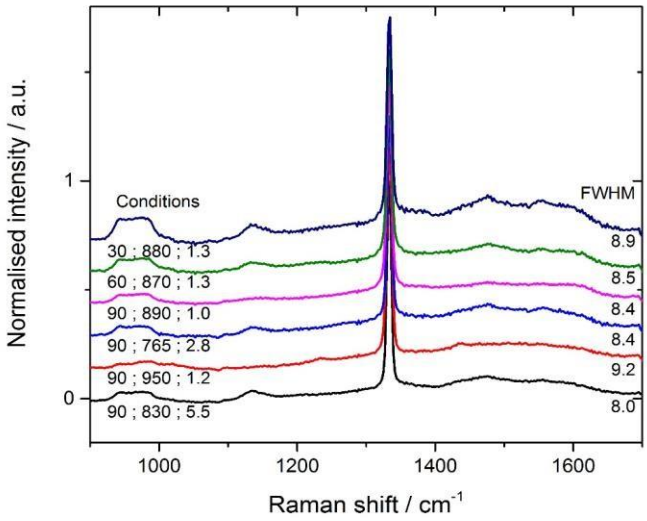

Figure 5: Raman spectra for the various samples deposited under static-mode conditions. The intensities are normalized to the height of the 1332 cm^{-1} diamond peak and a rigid shift of 0.15 a.u. has been applied to the intensity axis to separate the spectra. The labelling of each spectrum takes the form: {deposition time / min};{deposition temperature / °C};{leak rate / mtorr h^{-1}} at the left and {FWHM of the 1332 cm^{-1} peak / cm^{-1}} at the right.

3.4 Comparison of diamond growth under static- and flow-mode conditions

A further understanding of the static-mode deposition needs direct comparisons to be made with material grown by standard flow-mode methods. Therefore, additional flow-mode

experiments were conducted, at T_{sub} ~ 890°C, which sought to mimic the time-evolving plasma composition prevailing in the static-mode growth experiments. This was achieved by progressively reducing $F(CH_4)$ from a set starting point ($F(CH_4)_{init}$) to match the carbon content in the plasma core (as revealed by $I(C_2^*)$) over a 90 min period. The $F(CH_4)$ profile used is shown in the inset to Figure 6, which also shows the $I(C_2^*)$ vs t profiles measured for two different initial CH_4/H_2 mixing ratios, with $F(CH_4)_{init}$ corresponding to 6% (Flow A) and 5.4% (Flow B) of the total input. As Figure 6 shows, the $I(C_2^*)$ vs t profiles obtained with this tracked flow-mode procedure match well with that measured for static-mode growth at the same T_{sub}.

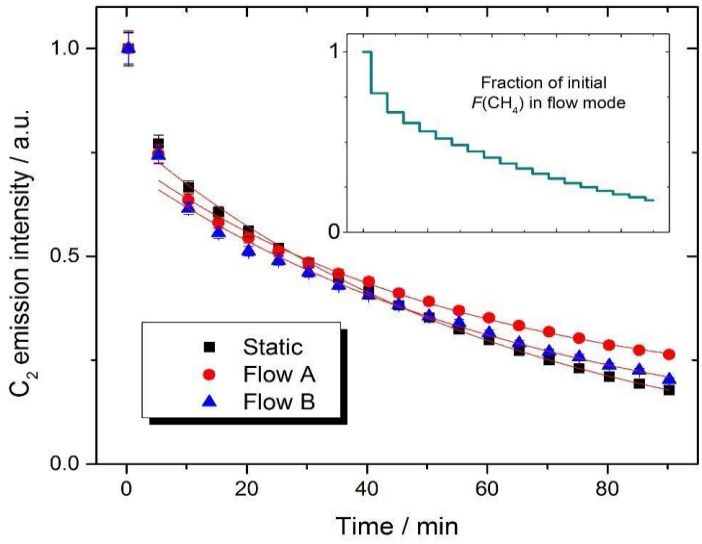

Figure 6: $I(C_2^*; z \sim 12$ mm) emission intensities measured as a function of time during two tracked flow-mode runs (red circles and blue triangles) compared with that for a static-mode run (black squares) at the same T_{sub} (~ 890°C). $F(CH_4)$ was adjusted every 5 minutes in the tracked flow-mode experiments to reduce the carbon content in the plasma core (as revealed by the $I(C_2^*)$ signal) to match that in the static-mode experiment. The initial CH_4 input mole fractions for the tracked flow-mode experiments were, respectively, 6% (Flow A) and 5.4% (Flow B) and the $F(CH_4)$ profile employed over the same time interval is shown in the inset.

OES confirms the similarity of the plasmas prevailing in static- and tracked flow-mode operation providing that, in the latter case, $F(CH_4)$ has the appropriate time dependence. As Figure 7 shows, the deposited films also show strong similarities. All films are polycrystalline, with facetted surfaces and no obvious morphological differences between the samples grown

under static- and tracked flow-mode conditions. The film grown under static-mode conditions is marginally thicker, hinting at a slightly higher deposition rate – possibly reflecting the slightly greater time-averaged nitrogen contamination (from the small reactor leak) under these conditions. Thus, from the perspectives of growth rate and material morphology also, there is little to indicate that low leak-rate, static-mode deposition is fundamentally inferior to flow-mode deposition under similar process conditions.

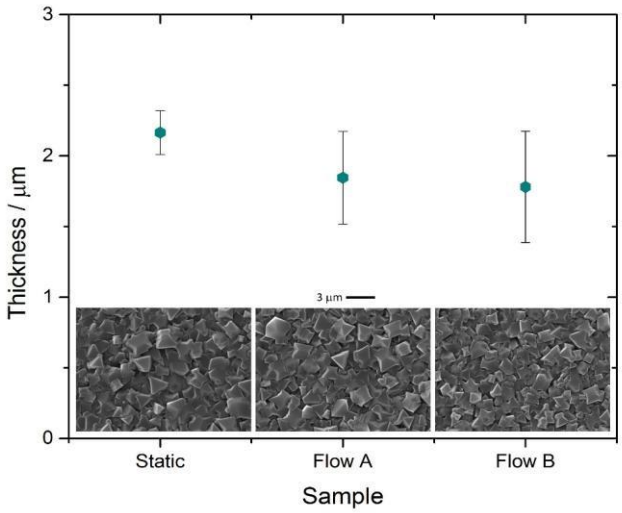

Figure 7: Thicknesses of diamond films grown by static- and tracked flow-mode operation along with plan view SEM images of the respective samples (insets).

This conclusion extends to the material quality also, as evidenced by the Raman spectra of the static- and tracked flow-mode samples shown in Figure 8. These reveal comparable sp^3 and sp^2 carbon ratios and very similar FWHM values for the strong 1332 cm^{-1} feature. Careful inspection of the SEM images in Figure 7 shows that the Flow B sample has a slightly smaller average grain size and the associated increase in surface grain boundary density probably accounts for the increased showing of the sp^2 carbon features in the Flow B spectrum. Thus, from the material quality perspective (as revealed by Raman spectroscopy) also, there appears to be little to discriminate between appropriately designed static- and flow-mode deposition methods.

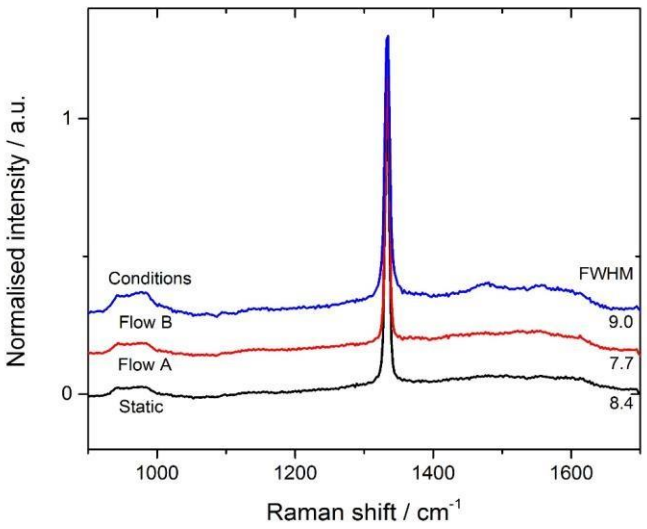

Figure 8: Raman spectra of samples grown using tracked flow-mode (Flow A and B) and static-mode conditions. The intensities are normalized to the height of the 1332 cm^{-1} diamond peak and a rigid shift of 0.15 a.u. has been applied to the intensity axis to separate the spectra. The respective FWHM values (in cm^{-1}) of the 1332 cm^{-1} peak are shown at the right.

The volumes of methane introduced into the reactor during static- and tracked flow-mode operation (Flow A and B) are, respectively, 27, 719 and 539 standard cm^3 – with the former calculated using the total sealed volume of 2.5 L. The molar quantity of input methane and diamond product was estimated assuming, in the former case, ideal gas behaviour and, in the latter, the density of bulk diamond (3.51 g m^{-3}) and a volume given by the product of the thickness and the nominal substrate area. These assumptions yield the following crude estimates of the percentage conversion of methane carbon to diamond carbon: ~5.8% for static-mode growth, and ~0.2% for tracked flow A or flow B modes at the same T_{sub} (~890°C), *i.e.* a factor of ~ 30 difference between the two. The conversion efficiency quoted for static-mode condition surely under-estimates what could be achieved with an extended deposition time *t* and an optimally designed reactor in which all of the input gas (*i.e.* if all of the gas residing in the voluminous exhaust line) was available for plasma processing near the substrate. But, even with this proviso, the present data clearly show that static-mode deposition (or an intelligent development therefrom) can offer a much greater process gas utilization efficiency than is achieved in research diamond CVD reactors such as the one used in this study.

4. Conclusions

This paper shows that diamond can be deposited on a silicon substrate using a MW plasma activated CH_4/H_2 gas mixture under zero-gas flow (or 'static-mode') conditions. The $I(C_2^*)$ optical emission intensity (a proxy for the total carbon content in the hot plasma core) was used to confirm that the time dependent loss of plasma carbon was linked to the thickness of the resulting diamond film. Faster gas phase carbon depletion rates correlated with growth of thicker diamond films. Both the loss of gas phase carbon and film thickness can be directly linked to growth parameters that are traditionally considered to affect diamond growth – principally substrate temperature, but also the level of nitrogen (air) impurity in the process gas mixture. The as-grown films display morphologies and Raman spectra typical of polycrystalline diamond, and experiments involving different growth times suggest that viable static-mode diamond growth conditions should extend beyond the maximum times (t = 90 min) investigated in the present work.

Direct comparison of static- and tracked flow-mode deposition (*i.e.* depositions carried out with a flowing process gas mixture in which $F(CH_4)$ is progressively reduced) emphasizes the similarities of the two modes and finds little difference between samples regarding their sp^3/sp^2 carbon content or crystalline morphology. Any differences identified are likely attributable to minor differences in process conditions, including the greater time-averaged nitrogen contamination of any static-mode process gas mixture. Carbon balance considerations indicate ~5.8% conversion of input gas phase carbon into diamond during the present t = 90 min deposition experiments at T_{sub} ~ 890°C. This is a ~30-fold improvement over that achieved using similar flow-mode conditions and could surely be enhanced further. This study presents a new approach to growing CVD diamond, offering improved atom efficiency and less release of undesirable greenhouse gases, which could be particularly advantageous for depositions involving limited, expensive, or hazardous feedstock gases.

Acknowledgements

The authors are grateful for financial support from the Engineering and Physical Sciences Research Council (EPSRC) through grant nos. EP/E017436/1, EP/K018388/1 and EP/K030302/1, the EPSRC Centre for Doctoral Training in Diamond Science and Technology (EP/L015315/1), Element Six Ltd, and to colleague Dr James Smith, for his many and varied contributions.

References

[1] P.W. May, Diamond thin films: a 21st-century material. Phil. Trans. R. Soc. A, 358 (2000) 473-495. doi:10.1098/rsta.2000.0542

[2] S.E. Coe, R.S. Sussmann, Optical, thermal and mechanical properties of CVD diamond. Diam. Rel. Mater. 9 (2000) 1726-1729. doi:10.1016/S0925-9635(00)00298-3

[3] P. Latawiec, V. Venkataraman, M.J. Burek, B.J.M. Hausmann, I. Bulu, M. Lončar, On-chip diamond Raman laser. Optica. 2 (2015) 924-928. doi:10.1364/OPTICA.2.000924

[4] P.J. Schlosser, D.C. Parrotta, V.G. Savitski, A.J. Kemp, J.E. Hastie, Intracavity Raman conversion of a red semiconductor disk laser using diamond. Opt. Express. 23 (2015) 8454-8461. doi:10.1364/OE.23.008454

[5] B. Dai, J. Zhao, V. Ralchenko, A. Khomich, A. Popovich, K. Liu, G.Y. Shu, G. Gao, S. Mingqi, L. Yang, P. Lei, J.C. Han, J.Q. Zhu, Thermal conductivity of free-standing CVD diamond films by growing on both nucleation and growth sides. Diam. Rel. Mater. 76 (2017) 9-13. doi:10.1016/j.diamond.2017.03.014

[6] S. Graham, Thermal Transport in Diamond Films for Electronics Thermal Defense Management, Accession Number AD1048799, Technical Report, Information Centre, US Government documentation, Georgia Institute of Technology, (2018).

[7] M.N.R. Ashfold, E.J.D. Mahoney, S. Mushtaq, B.S. Truscott, Yu.A. Mankelevich, What

[plasma used for growing] diamond can shine like flame? Chem. Comm. 53 (2017) 10482-10495. doi: 10.1039/c7cc05568d

[8] M. Craciun, C.H. Saby, P. Muret, A. Deneuville, A 3.4 eV potential barrier height in Schottky diodes on boron-doped diamond thin films, Diam. Rel. Mater., 13 (2004) 292-295. doi: 10.1016/j.diamond.2003.10.012

[9] C.J. Tang, A.J.S. Fernandes, M. Granada, J.P. Leitão, S. Pereira, X.F. Jiang, J.L.Pinto, H. Ye, High rate growth of nanocrystalline diamond films using high microwave power and pure nitrogen/methane/hydrogen plasma. Vacuum. 122 (2015) 342-346. doi: 10.1016/j.vacuum.2015.03.021

[10] A.P. Bolshakov, V.G. Ralchenko, V.Y. Yurov, A.F. Popovich, I.A. Antonova, A.A. Khomich, E.E. Ashkinazi, D.N. Sovyk, I.A. Antonova, S.S. Savin, V.V. Voronov, M.Y. Shevchenko, B. dai, J. Zhu, High-rate growth of single crystal diamond in microwave plasma in CH_4/H_2 and $CH_4/H_2/Ar_2$ gas mixtures in presence of intensive soot formation. Diam. Rel. Mater. 62 (2016) 49-57. doi: 10.1016/j.diamond.2019.107466

[11] J.E. Butler, Yu.A. Mankelevich, A. Cheesman, J. Ma, M.N.R. Ashfold, Understanding the chemical vapor deposition of diamond: recent progress. J. Phys. Condens. Matter 21 2009 364201. doi:10.1088/0953-8984/21/36/364201

[12] Yu.A. Mankelevich, M.N.R. Ashfold, J. Ma, Plasma-chemical processes in microwave plasma-enhanced chemical vapor deposition reactors operating with C/H/Ar gas mixtures J. Appl. Phys. 104 (2008) 113304. doi: 10.1063/1.3035850

[13] N. Derkaoui, C. Rond, K. Hassouni, A. Gicquel, Spectroscopic analysis of H_2/CH_4 microwave plasma and fast growth rate of diamond single crystal. J. Appl. Phys. 115 (2014) 233301. doi:10.1063/1.4883955

[14] G. Lombardi, K. Hassouni, G.D. Stancu, L. Mechold, J. Röpcke, A. Gicquel, Study of an H_2/CH_4 moderate pressure microwave plasma used for diamond deposition: modelling and IR tuneable diode laser diagnostic. Plasma Sources Sci. Technol. 14 (2005) 440-450. doi:10.1088/0963-0252/14/3/005

[15] J.R. Rabeau, P. John, J.I.B. Wilson, Y. Fan, The role of C_2 in nanocrystalline diamond growth. J. Appl. Phys. 96 (2004) 6724-6732. https://doi.org/10.1063/1.1810637

[16] B.S. Truscott, M.W. Kelly, K.J. Potter, M.N.R. Ashfold, Yu.A. Mankelevich, Microwave plasma-activated chemical vapour deposition of nitrogen-doped diamond, II: $CH_4/N_2/H_2$ plasmas. J. Phys. Chem. A, 120 (2016) 8537-8549. doi:10.1021/acs.jpca.6b09009

[17] J.C. Richley, M.W. Kelly, M.N.R. Ashfold, Optical Emission from Microwave Activated C/H/O Gas Mixtures for Diamond Chemical Vapor Deposition. J. Phys. Chem. A. 116 (2012) 9447-9458. doi:10.1021/jp306191y

[18]S. Jin, T.D. Moustakas, Effect of nitrogen on the growth of diamond films. Appl. Phys. Lett. 65 (1994), 403-405. doi: 10.1063/1.112315

[19]W. Müller-Sebert, E. Wörner, F. Fuchs, C. Wild, P. Koidl, Nitrogen induced increase of growth rate in chemical vapor deposition of diamond. Appl. Phys. Lett. 68 (1996) 759-760. doi:10.1063/1.116733

[20]A. Chayahara, Y. Mokuno, Y. Horino, Y. Takasu, H. Kato, H. Yoshikawa, N. Fujimori, The effect of nitrogen addition during high-rate homoepitaxial growth of diamond by microwave plasma CVD. Diam. Rel. Mater. 13 (2004) 1954-1958. doi:10.1016/j.diamond.2004.07.007

[21]J. Achard, F. Silva, O. Brinza, A. Tallaire, A. Gicquel, Coupled effect of nitrogen addition and surface temperature on the morphology and the kinetics of thick CVD diamond single crystals. Diam. Rel. Mater. 16 (2007) 685-689. doi.10.1016/j.diamond.2006.09.012

[22]S. Bogdanov, A. Vikharev, A. Gorbachev, A. Muchnikov, D. Radishev, N. Ovechkin, V. Parshin, Growth-rate Enhancement of High-quality, Low-loss CVD-produced Diamond Disks Grown for Microwave Windows Application. Chem. Vapor Depos. 20 (2013) 32-38. doi:10.1002/cvde.201307058

[23]T. Kawato, K. Kondo, Effects of Oxygen on CVD Diamond Synthesis. Jap. J. Appl. Phys. 26 (1987) 1429-1432

[24]S.J. Harris, A.M. Weiner, Effects of Oxygen on Diamond Growth. MRS Proceedings. 162 (1989) 103-108. doi.org/10.1557/PROC-162-103

[25]Y. Muranaka, H. Yamashita, K. Sato, H. Miyadera, The role of hydrogen in diamond synthesis using a microwave plasma in a CO/H_2 system. J. Appl. Phys. 67 (1990) 6247-6254. doi:10.1143/JJAP.26.1429

[26]W. Chen, X. Lu, Q. Yang, C. Xiao, R. Sammynaiken, J. Maley, A. Hirose, Effects of gas flow rate on diamond deposition in a microwave plasma reactor. Thin Solid Films, 515 (2006) 1970–1975. doi:10.1016/j.tsf.2006.08.007

[27]V. Ralchenko, I. Sychov, I. Vlasov, A. Vlasov, V. Konov, A. Khomich, S. Voronina, Quality of diamond wafers grown by microwave plasma CVD: effects

of gas flow rate. Diam. Rel. Mater. 8 (1999) 189–193.doi:10.1016/S0925-9635(98)00427-0

[28]F.G. Celii, Jr. D. White, A.J. Purdes, Effect of residence time on microwave plasma chemical vapor deposition of diamond. J. Appl. Phys. 70 (1991) 5636–5646. doi:10.1063/1.350179

[29]F.G. Celii, Jr., D. White, A.J. Purdes, Deposition of smooth, oriented diamond films using microwave plasma chemical vapor deposition. Thin Solid Films, 212 (1992) 140–149. doi:0.1016/0040-6090(92)90512-A

[30]J. Su, Y. Li, Y. Liu, M. Ding, W. Tang, Revisiting the gas flow rate effect on diamond films deposition with a new dome-shaped cavity type microwave plasma CVD reactor. Diam. Rel. Mater. 73 (2017) 99–104. doi:10.1016/j.diamond.2016.07.014

[31]S.V. Nistor, M. Stefan, V. Ralchenko, A.V. Khomich, D. Schoemaker, Nitrogen and Hydrogen in thick diamond films grown by microwave plasma enhanced chemical vapor deposition at variable H_2 flow rates. J. Appl. Phys. 87 (2000) 8741–8746. doi:10.1063/1.373604

[32]L.F. Hei, J. Liu, C.M. Li, J.H. Song, W.Z. Tang, F.X. Lu, Fabrication and characterizations of large homoepitaxial single crystal diamond grown by DC arc plasma jet CVD. Diam. Rel. Mater. 30 (2012) 77-84. doi:10.1016/j.diamond.2012.10.002

[33]I.A. Martorell, W.D. Partlow, R.M. Young, J.J. Schreurs, H.E. Saunders, Gas recycling and flow control for cost reduction of diamond films deposited by DC arc-jet. Diam. Rel. Mater. 8 (1991) 29-36. doi:10.1016/S0925-9635(98)00298-2

[34]W. Tang, J. Liu, T. Huang, F. Lu, Preparation of diamond wafers by DC arc jet plasma process under a gas recycling mode, Diam. Rel. Mater. 10 (2001) 327-331. doi: 10.1016/S0925-9635(00)00592-6

[35]K. Snail, High temperature, high rate, epitaxial synthesis of diamond in a laminar plasma, US patent; 5,704,976, 1998.

[36]J. Ma, M.N.R. Ashfold, Yu.A. Mankelevich, Validating optical emission spectroscopy as a diagnostic of microwave activated $CH_4/Ar_2/H_2$ plasmas used for

diamond chemical vapor deposition. J. Appl. Phys. 105 (2009) 043302. doi:10.1063/1.3078032

[37] E.J.D. Mahoney, B.S. Truscott, M.N.R. Ashfold, Yu.A. Mankelevich, Optical Emission from C_2^- Anions in Microwave-Activated CH_4/H_2 Plasmas for Chemical Vapor Deposition of Diamond. J. Phys. Chem. A. 121 (2017) 2760-2772. doi:10.1063/1.3078032

[38] A. Croot, G. Wan, A. Rowan, H.D. Andrade, J.A. Smith, N.A. Fox Beta Radiation Enhanced Thermionic Emission from Diamond Thin Films, Front. Mech. Eng., 3 (2017) 17-25 . doi.org/10.3389/fmech.2017.00017

[39] C.M. Western, PGOPHER: A program for simulating rotational, vibrational and electronic spectra, Journal of Quantitative Spectroscopy and Radiative Transfer, 186 (2017) 221-242 doi:10.1016/j.jqsrt.2016.04.010

[40] E. J. D. Mahoney, B. J. Rodriguez, S. Mushtaq, B. S. Truscott, M. N. R. Ashfold, Y. A. Mankelevich, Imaging and Modelling the Optical Emission from CH Radicals in Microwave Activated C/H Plasmas J. Phys. Chem. A, 123 (2019) 9966-9977, doi:10.1021/acs.jpca.9b08345